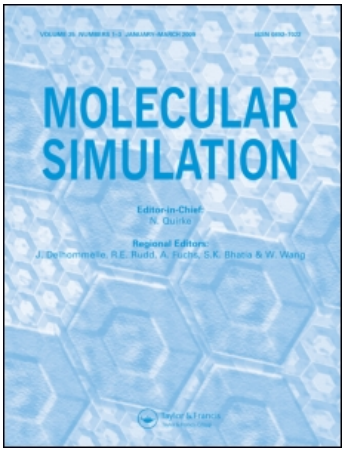

Molecular Simulation
Publication details, including instructions for authors and subscription information:
http://www.informaworld.com/smpp/title~content=t713644482

The study of the electronic structures and properties of pure and transition metal-doped silicon nanoclusters: a density functional theory approach

Debashis Bandyopadhyay[a]
[a] Department of Physics, Birla Institute of Technology and Science, Pilani, India

To cite this Article Bandyopadhyay, Debashis(2009) 'The study of the electronic structures and properties of pure and transition metal-doped silicon nanoclusters: a density functional theory approach', Molecular Simulation, 35: 5, 381 — 394
To link to this Article: DOI: 10.1080/08927020802603598
URL: http://dx.doi.org/10.1080/08927020802603598

Molecular Simulation
Vol. 35, No. 5, April 2009, 381–394

Taylor & Francis
Taylor & Francis Group

The study of the electronic structures and properties of pure and transition metal-doped silicon nanoclusters: a density functional theory approach

Debashis Bandyopadhyay*

Department of Physics, Birla Institute of Technology and Science, Pilani, India

(*Received 15 April 2008; final version received 5 November 2008*)

This report presents the study of *ab initio* electronic structure and properties of pure and transition metal (TM = Ti, Zr and Hf)-doped silicon clusters, TM@Si(n), by using density functional theory with a polarised basis set (LanL2DZ) within the spin-polarised generalised gradient approximation for different values of n varying from 8 to 20. As the first step of the study, different optimised geometries of pure and doped clusters are calculated. These optimised clusters are then used to calculate different structural and physical parameters of the clusters, like binding energy, Highest Occupied Molecular Orbital – Lowest Unoccupied Molecular Orbital (HOMO–LUMO) gap, charge transfer, etc. In order to check the stability of the clusters, the second-order difference in the energy of the optimised structures is calculated. To study the optical behaviour of the clusters, infrared and Raman spectra are also calculated. Further calculations are also done on cation and anion clusters of both pure and doped nanoclusters to obtain their ionisation potential, electron affinity and chemical potential. An effort has been made to correlate the variation of different calculated parameters with the size of the clusters to explain the real existence and stabilities of different TM-doped clusters.

Keywords: *ab initio*; DFT; nanoclusters; binding energy; stability; charge transfer; I.P; E.A; IR and Raman

1. Introduction

For the last two decades, the theoretical as well as experimental study of the electronic structures and properties of two to a few hundred atomic clusters has shown a new phase of matter, where the properties are different from those of individual atoms as well as the bulk matter [1]. In particular, the study of semiconductor nanoclusters is an interesting and active area of research due to its importance in nanoscience and nanotechnology. Recent investigation [2–8] of the metal-doped silicon and germanium clusters has been undertaken with much interest to understand their properties and growth behaviour [9–17]. These properties are attractive for reducing the size of the different electronic devices useful in optoelectronic, magnetic, sensor, catalytic and in other different fields. Hiura et al. [3] reported the experimental evidence of a series of silicon cage clusters with transition metal (TM) atoms Hf, Ta, W, Re, Ir, etc., with a very large abundance of the size of the clusters with $n = 15$ and 16. Experimental evidence of a large abundance of TM@Si_n ($n = 15$ and 16, TM = Ti, Hf, Cr, Mo and W) clusters, in addition to the relatively low abundance of other silicon clusters [17–19], first supported the theoretical prediction on the metal-doped silicon clusters. Ohara et al. [17,18] studied the geometric and electronic structures of the pure and negatively charged Ti-doped Si_n clusters for $6 \leq n \leq 16$ with photoelectron spectroscopy and chemical probe method, and proved that the Ti atom always remains encapsulated inside the silicon clusters with size $n \geq 10$. The drastic drop in the abundances of silicon clusters beyond $n = 16$ supports the predictions of the exceptional stability of $n = 16$ clusters. The electronic structures of Ti-doped silicon clusters have been studied recently with photoelectron spectroscopy and it has been found that the closed electronic shell nature clusters with $n = 16$ have strong stability when doped with Ti. Electroluminescence emission of crystalline silicon nanoclusters grown at a low temperature was studied by Tsai et al. [20]. In another study, Comedi et al. [21] reported the X-ray diffraction results of the formation of silicon nanoclusters. They reported the dependence of the size of the silicon nanoclusters on the annealing temperature and time. The measured activation energy value of their experiment agrees with the reported activation energy value obtained by transmission electron microscopy. They observed a photo-luminescence band below 1.7 eV. Liu et al. [22] reported a critical theoretical study on the factors responsible for the stability and the clean band gap in silicon nanoclusters. Extensive studies have been made by Kumar and Kawazoe [23] on the growth and structural behaviour of metal-doped Si_n ($n = 14–20$) clusters. Kawamura et al. [24,25] reported that silicon forms fullerene-like Si16 structure when it is doped with Hf and Zr, or cubic Si_{14} structure when doped with Fe, Ru and Os clusters. In a recent study, Bandyopadhyay [26] has obtained the results of the growth

*Emails: bandy@bits-pilani.ac.ac.in; rajuban@gmail.com

ISSN 0892-7022 print/ISSN 1029-0435 online

DOI: 10.1080/08927020802603598
http://www.informaworld.com

behaviour of the silicon system, which agree with those obtained by Kawamura et al. [24,25]. Keeping the recent progress made in the field of nanoscience and technology in mind, much attention is paid in the present work to the study of the different properties of TM@Si(n) ($n = 10$–20, TM = Ti, Zr and Hf) nanoclusters. After optimisation of different guess geometries, the ground-state optimised structures are then used to calculate the binding energy (B.E.), HOMO–LUMO gap (ΔE), ionisation potentials (I.Ps.), electron affinities (E.As.) and chemical potentials. To check the optical properties of the clusters, infrared (IR) and Raman spectra are also calculated.

2. Methodology

Density functional theory (DFT) is used to optimise different TM@Si(n) nanoclusters. Self-consistent-field (SCF) electronic structure calculations are carried out on all clusters. Calculations are performed with the DFT in the spin-polarised generalised gradient approximation using the Perdew–Wang exchange and Perdew–Wang 91 correlation [27–31] with a LanL2DZ basis set, which is very effective as core potential with no symmetry constraint. This provides an effective way to reduce the difficulties in two-electron integrals caused by the heavy TM atoms [32–35]. The optimised electronic structures are obtained by solving the Kohn–Sham equations self-consistently. Geometry optimisations are carried out with a convergence limit of 10^{-7} Hartree on the total electronic energy. The optimised electronic structure for each cluster is obtained from the Z-matrices in the program output while electronic properties are calculated from the SCF total electronic energy and from the orbital energy values. All theoretical calculations are performed with GAUSSIAN-98 program package [36]. The optimisation of the structures are reassured accurately by checking harmonic vibrational frequency calculation (IR and Raman). If an imaginary vibrational mode is found, a relaxation along coordinates of imaginary vibrational mode is carried out until the true local minimum is actually obtained.

3. Results and discussion

Optimised structures of different pure and TM-doped silicon clusters are shown in Figures 1 and 2, respectively, with n varying from 7 to 20. Only the lowest energy ground-state structures of TM@Si(n) are presented in Figure 2, where TM represents the TMs Ti, Zr and Hf. Calculated physical parameters of these structures, like binding energies, HOMO–LUMO gap, dipole moment, etc., are shown in Tables 1 and 2. Different optimised structures calculated in the present work will be discussed in the following section.

3.1 Structural and growth behaviour of pure and metal-doped silicon clusters for n = 7–20

3.1.1 n = 7

The smallest size pure silicon structure for $n = 7$ and five different optimised geometries with different point groups are found. Among them, the structure named Si7(A) shown in Figure 1 is the lowest energy ground-state isomer with maximum bond length 2.76 Å. This is a bicapped pentagonal structure with D_{5h} symmetry group. The calculated HOMO–LUMO gap of this cluster (3.27 eV) is much higher than the other clusters in this family of pure clusters with $n = 7$. Moreover, the structural symmetry of this ground-state cluster shows minimum dipole moment of 0.003 D. Different parameters of the other members of this group are shown in Table 1. The B.E. of the ground-state clusters is 4.11 eV per atom and this is higher than the other clusters in the family. Since the size of this cluster is small, it cannot absorb any TMs endohedrally under the present calculations, but it can absorb metal atom on its surface, which is not the interest of the present study.

3.1.2 n = 8

For $n = 8$, eight different optimised structures with different point groups are found and are shown in Figure 1. The ground-state isomer in this family is the structure shown in Figure 1 by Si8(A) with C_{2v} symmetry group. It has an average bond length of 2.67 Å with a HOMO–LUMO gap of 2.38 eV. This structure of this cluster could be obtained by adding four silicon atoms at the four planes of a trigonal pyramidal structure in Si4. The dipole moment of this cluster is 0.496 D, which is higher than the most stable cluster Si7(A) in the last group. It has a B.E. value of 4.07 eV, which is lower than the Si7(A) cluster, but the average B.E. is higher than the family of clusters with $n = 7$. Encapsulation of the TM atoms is first tried for this structure. It cannot absorb any TM atoms endohedrally. Therefore, a new kind of bowl-like structure with three walls is used to capture the TM atom and is shown in Figure 2. Therefore, this structure can hold the TM atom externally.

3.1.3 n = 9

Four different optimised structures are found for Si9 clusters as shown in Figure 1. Energetically favourable, the most stable structure, Si9(A), has an average bond length of 2.65 Å with a HOMO–LUMO gap of 3.05 eV and has C_{2v} symmetry. The dipole moment of this cluster is 0.337 D, which is higher than the most stable cluster in Si7 group. The B.E. of the clusters is shown in Table 2. It is higher than the ground-state B.E. of previous clusters. The average B.E. is also higher than the average B.E. of the clusters in the family with $n = 7$ and 8.

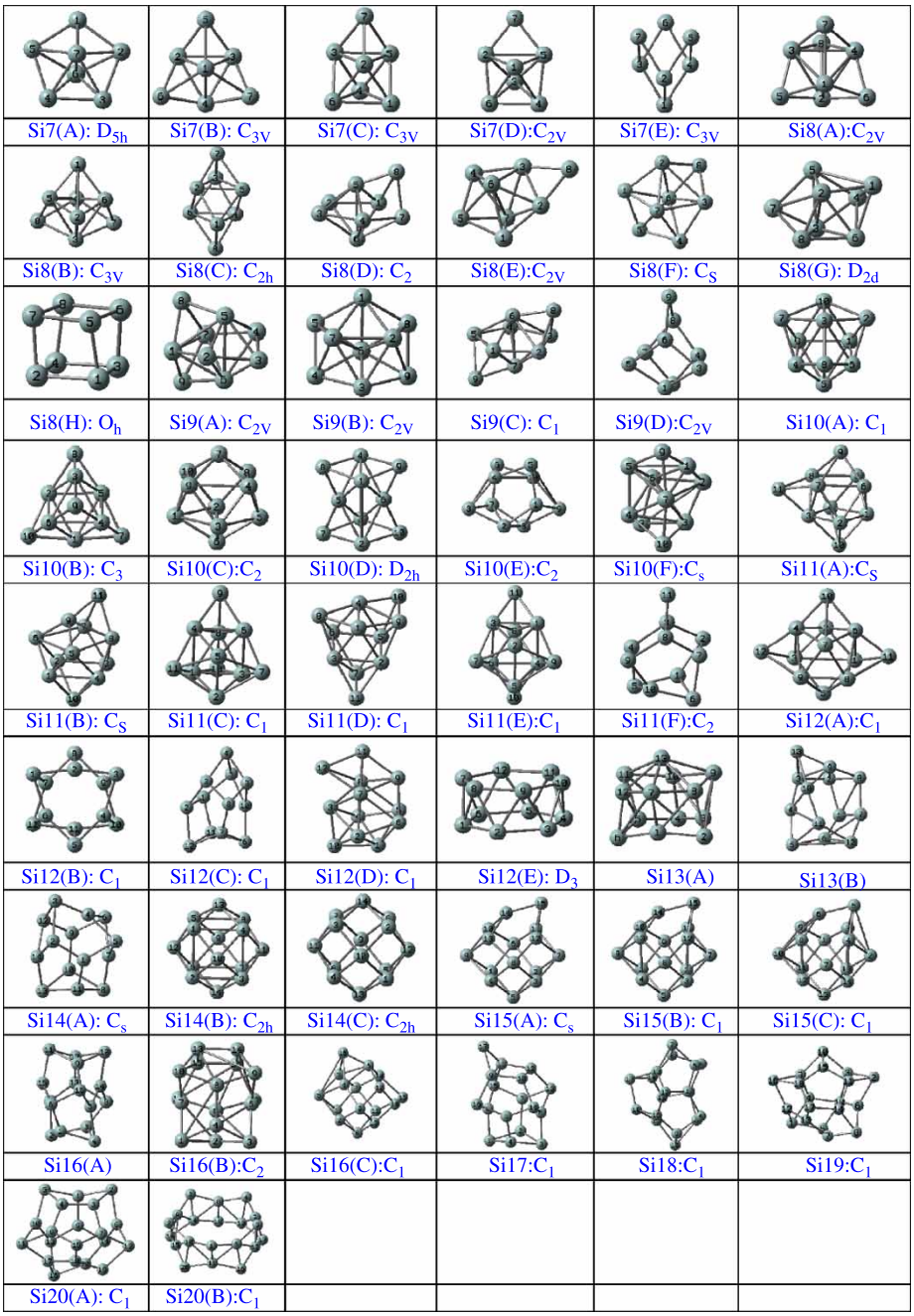

Figure 1. Optimised structure of silicon clusters $n = 7–20$.

It is relevant to mention here the work reported by Kawamura et al. [25] on the encapsulation of metal in pure silicon clusters. It is clear that to enclose a molecule, a three-dimensional cage-like structure is needed. Therefore, optimisation with the encapsulated metal atom has started in the present work with Si8 clusters. However, it is found that in a small-sized isomer, a cage-like structure is not favourable and therefore such an isomer cannot enclose or hold a guest TM atom inside. In the present study, TM atoms (Ti, Zr and Hf) are put inside different Si8 and Si9 clusters, but in both the cases the encapsulated Si clusters are found unstable. The transitions metal atoms cannot stay inside the Si structure cage. The enclosed guess structures finally break and absorb the guest atoms on its surface. The optimised structures of Si8 and Si9 doped with Ti atom are shown in Figure 2. The HOMO–LUMO orbital distribution of the ground-state isomer Si9(A)Ti is shown in Figure 3. The HOMO–LUMO distributions are well extended from the region of silicon atoms (i.e. surface of the cage) to the doped titanium.

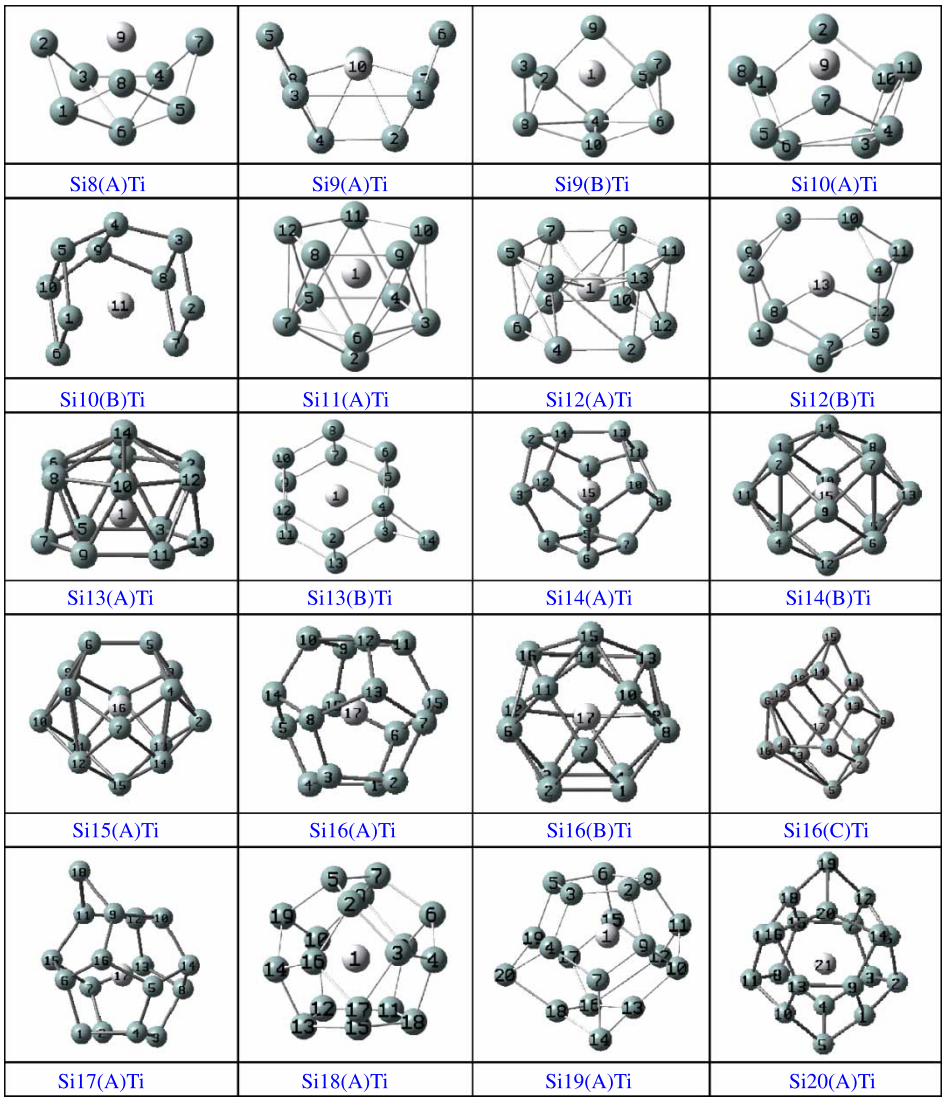

Figure 2. Optimised structure of Si(n)Ti clusters for $n = 8–20$.

This is true for LUMO also. The shape of both the distributions is symmetrical when projected by keeping the titanium atom at the central position of the plane of the figure as shown. From the HOMO distribution, the non-zero value of the dipole moment can be understood, which is 0.40 D in Si9(A)Ti. In the optimised cluster, the guest TM atoms are negatively charged in both Si9(A)Ti and Si9(B)Ti clusters. The host atoms in the cage are always holding positive charges of different amount.

3.1.4 n = *10*

For the pure Si10 cluster, six different optimised structures are found as shown in Figure 1. The most stable structure, Si10(A), has an average bond length 2.68 Å with a band gap of 3.02 eV. The dipole moment of this cluster is 0.374 D, which is higher than the other stable cluster in this group. B.E. of the clusters is 4.28 eV, which is also higher than the other neighbouring clusters. In Si10 cluster, the average B.E. is also higher than that of the smaller clusters. The two clusters Ti@Si10(A) and Ti@Si10(B) as shown in Figure 2 are the first members in the present calculation that can hold the TM atoms exhedrally and without much distortion in the initial guess structure. Among these two types of structures, TM@Si10(A) is always energetically favourable and can be taken as ground-state cluster. This is a combination of two pentagons and two quadrilaterals. It is well known that pentagon and quadrilateral combinations always reduce the unbalanced strain and give more stability to the structure [25]. In TM@Si10(B) cluster, two open pentagons are connected parallel to each other.

Table 1. Different parameters of pure silicon clusters.

Clusters $n = 7–20$	Moment (D)	B.E. (eV)	ΔE (eV)	Average ΔE^n (eV) Neutral	Average ΔE^n (eV) Cation	Average ΔE^n (eV) Anion	E.A. (eV)	I.P. (eV)
Si7(A)	0.003	4.12	3.271	Not applicable	Not applicable	Not applicable	2.251	7.789
Si7(B)	0.225	4.04	3.163					
Si7(C)	0.815	3.90	2.161					
Si7(D)	1.325	3.88	2.256					
Si7(E)	0.823	3.90	2.172					
Si8(A)	0.496	4.07	2.386	−0.561	−0.096	−1.043	2.119	7.650
Si8(B)	0.492	4.07	2.389					
Si8(C)	0.005	4.06	2.557					
Si8(D)	0.849	4.02	2.388					
Si8(E)	0.207	4.00	1.880					
Si8(F)	0.328	3.99	1.922					
Si8(G)	1.056	4.01	2.339					
Si8(H)	0	3.86	1.303					
Si9(A)	0.337	4.17	3.049	−0.230	−0.646	0.195	2.468	7.677
Si9(B)	0.398	4.10	3.040					
Si9(C)	0.422	4.08	2.274					
Si9(D)	2.096	4.08	2.134					
Si10(A)	0.709	4.28	3.012	1.104	−0.575	1.390	2.230	7.838
Si10(B)	0.004	4.23	3.682					
Si10(C)	0.002	4.16	2.213					
Si10(D)	0.005	4.1	2.775					
Si10(E)	0.374	4.23	2.509					
Si10(F)	0.888	4.21	2.698					
Si11(A)	1.042	4.220	2.080	0.461	1.884	−0.804	2.030	7.309
Si11(B)	1.118	4.189	2.308					
Si11(C)	1.553	4.188	2.372					
Si11(D)	1.560	4.203	2.839					
Si11(E)	0.466	4.153	2.093					
Si11(F)	1.018	4.211	2.402					
Si12(A)	1.739	4.22	1.636	−1.171	0.794	0.024	2.935	7.297
Si12(B)	0.030	4.2	1.832					
Si12(C)	0.816	4.201	2.80					
Si12(D)	2.78	4.167	2.433					
Si12(E)	0.000	3.92	1.170					
Si13(A)	0.334	4.21	2.706	0.639	−0.864	−0.484	2.447	7.39
Si13(B)	0.681	4.15	1.981					
Si14(A)	1.311	4.27	1.964	−0.784	−0.927	0.562	3.478	7.508
Si14(B)	0	4.13	1.011					
Si14(C)	0	4.13	1.011					
Si15(A)	1.448	4.22	2.222	−0.579	−1.01	−0.876	2.965	7.480
Si15(B)	1.447	4.22	2.218					
Si15(C)	1.448	4.22	2.220					
Si16(A)	1.842	4.33	1.837	0.686	1.282	−0.036	2.749	7.022
Si16(B)	2.518	4.33	2.253					
Si16(C)	1.298	4.23	2.024					
Si17(A)	3.406	4.32	1.835	0.312	0.037	0.897	3.255	7.160
Si18(A)	1.846	4.33	1.735	0.044	0.165	−0.107	3.176	7.023
Si19(A)	0.653	4.33	1.665	−0.795	−0.815	−0.519	3.249	7.007
Si20(A)	0.629	4.38	1.850	N/A	N/A	N/A	3.045	6.972

Clusters named with italic letters are in ground state.

This structure is a like an open bucket, where the first one is like an open cage. The different parameters presented in Table 2 show that the B.E. of the first structure is more, where the band gap is higher in the second structure. The HOMO–LUMO distributions in both the doped clusters are shown in Figure 3. Both HOMO and LUMO distributions are extended inside as well as outside the cage. The HOMO distribution in Si10(A)Ti is symmetrical about the doped atom. In both the clusters, the guest atom is always negative. From the HOMO–LUMO distributions, it can be understood why the small cage like Si9 and Si10 cannot hold the guest atom inside.

Table 2. Different parameters of TM-doped silicon clusters.

Clusters	Moment (D)	ΔE (eV)	B.E. (eV)
Si_{10}(A)Ti	0.82	1.84	4.46
Si_{10}(B)Ti	0.02	2.04	4.44
Si_{10}(A)Zr	1.57	1.73	4.54
Si_{10}(B)Zr	0.15	1.88	4.59
Si_{10}(A)Hf	1.55	1.90	4.53
Si_{10}(B)Hf	0.08	1.70	4.55
Si_{12}(A)Ti	0.86	2.16	4.65
Si_{12}(B)Ti	0.68	2.43	4.56
Si_{12}(A)Zr	1.15	1.93	4.64
Si_{12}(B)Zr	1.16	1.97	4.63
Si_{12}(A)Hf	0.63	2.15	4.68
Si_{12}(B)Hf	0.67	2.17	4.68
Si_{14}(A)Ti	0.11	1.15	4.76
Si_{14}(B)Ti	0.08	2.26	4.60
Si_{14}(A)Zr	0.02	1.11	4.60
Si_{14}(B)Zr	2.10	2.13	4.76
Si_{14}(A)Hf	0.04	1.07	4.79
Si_{14}(B)Hf	0.03	2.16	4.59
Si_{15}(A)Ti	0.46	2.55	4.70
Si_{15}(A)Zr	0.55	2.58	5.25
Si_{15}(B)Hf	0.55	2.54	4.74
Si_{16}(A)Ti	0.01	2.36	4.88
Si_{16}(B)Ti	0.14	3.21	4.67
Si_{16}(A)Zr	0.00	2.34	5.45
Si_{16}(B)Zr	0.00	3.03	5.19
Si_{16}(A)Hf	0.00	3.00	4.96
Si_{16}(B)Hf	2.22	3.00	4.71
Si_{17}(A)Ti	0.85	1.80	4.83
Si_{17}(A)Zr	0.48	1.92	5.37
Si_{17}(A)Hf	0.49	1.90	4.91
Si_{18}(A)Ti	0.83	1.67	4.82
Si_{18}(A)Zr	0.61	1.67	5.33
Si_{18}(A)Hf	0.70	1.67	4.89
Si_{19}(A)Ti	3.76	1.84	4.78
Si_{19}(A)Zr	0.55	1.22	5.28
Si_{19}(A)Hf	0.49	1.20	4.86
Si_{20}(A)Ti	2.95	1.61	4.81
Si_{20}(A)Zr	3.60	1.45	5.29
Si_{20}(A)Hf	3.56	1.48	4.89

3.1.5 n = *11*

For the Si11 cluster, three different optimised structures are obtained. The most stable structure, Si11(A), of average bond length 2.61 Å with a HOMO–LUMO gap of 2.08 eV, is shown in Figure 1. The average dipole moment of these clusters is 1.126 D, whereas the highest value of the dipole moment in this series is 1.56 D for Si11(D). The B.E. of Si11(A) is higher than the other clusters in this series of value 4.22 eV as shown in Table 1. As with Si10, in the Si11 cluster the average B.E. is higher than the average B.E. of the smaller clusters as discussed, but it is very much closer to the average B.E. of the Si10 clusters. From the B.E. value given in Table 1, it is clear that the average B.E. value Si10 cluster is higher than its neighbouring clusters. The TM-doped Si11(A) cluster can be taken as the first host that can partly enclose the guest atom. The doped structure is like a tube with one side having a pentagonal and the other side having a hexagonal cross section with the endohedrally doped TM atom at the central region of the tube. HOMO–LUMO distributions are mostly extended on the surface region of the structure. All endohedrally doped atoms are negatively charged in the optimised structure.

3.1.6 n = *12*

For the Si12 group, calculated optimised structure is shown in Figure 1. There are four different optimised structures obtained for $n = 12$. The ground-state optimised structures are hexagonal basket kinds of structure with average bond length 2.47 Å and a HOMO–LUMO gap of energy 1.64 eV. The cluster Si12(E) is more like a hexagonal tube kind of structure with zero dipole moment. A little modification after adding two Si atoms with TM@Si10(A) above pentagonal plane as a capped atom gives TM@Si12(A). On the other hand, addition of Si atoms with TM@Si10(B) gives TM@Si12(B) optimised structure. Optimisation of these structures shows that TM@Si12(A) is a ground-state cluster. The average Si–TM and Si–Si bond lengths in TM(A)@Si12 are 2.62 and 2.689 Å, respectively. Other parameters of these structures are presented in Table 2. The HOMO–LUMO distribution in the ground-state titanium-doped cluster is symmetrically distributed surrounding the doped titanium as well as the silicon atoms in the host molecular structure. The space inside this tube structure can easily accommodate the guest atom inside the cluster. The doped structure is bigger than the undoped cluster and its B.E. as well as stability is also higher than the pure Si12 cluster.

3.1.7 n = *13*

Two different kinds of pure silicon structure are found for $n = 13$. The ground-state cluster can be obtained by adding one silicon with one surface of the hexagonal basket-like structure, Si12(E), as shown in Figure 1. Addition of one silicon atom on the curved surface of Si12(E) structure gives Si13(B) structure. The first structure can hold a guest atom. The calculated Ti-doped Si13(A) cluster is a one-sided capped tube with hexagonal cross-sectional planes. The hexagon which is closer to the capped silicon atom is smaller in area than the other one. The average diameter of the bigger hexagonal cross section is 5.15 Å and the lower one has a diameter of 5.08 Å. The average bond length between Si–Si bonds in the hexagonal rings is 2.63 Å and the same between the capped silicon atom and the upper hexagonal structure is 2.88 Å. These lengths are bigger than the average bond length in Si–Si bond in undoped Si13 cluster. The average Si–Ti bond length between the Si in the upper hexagon is 2.94 Å whereas the same between the Ti and lower hexagon is 2.71 Å. The bonding between

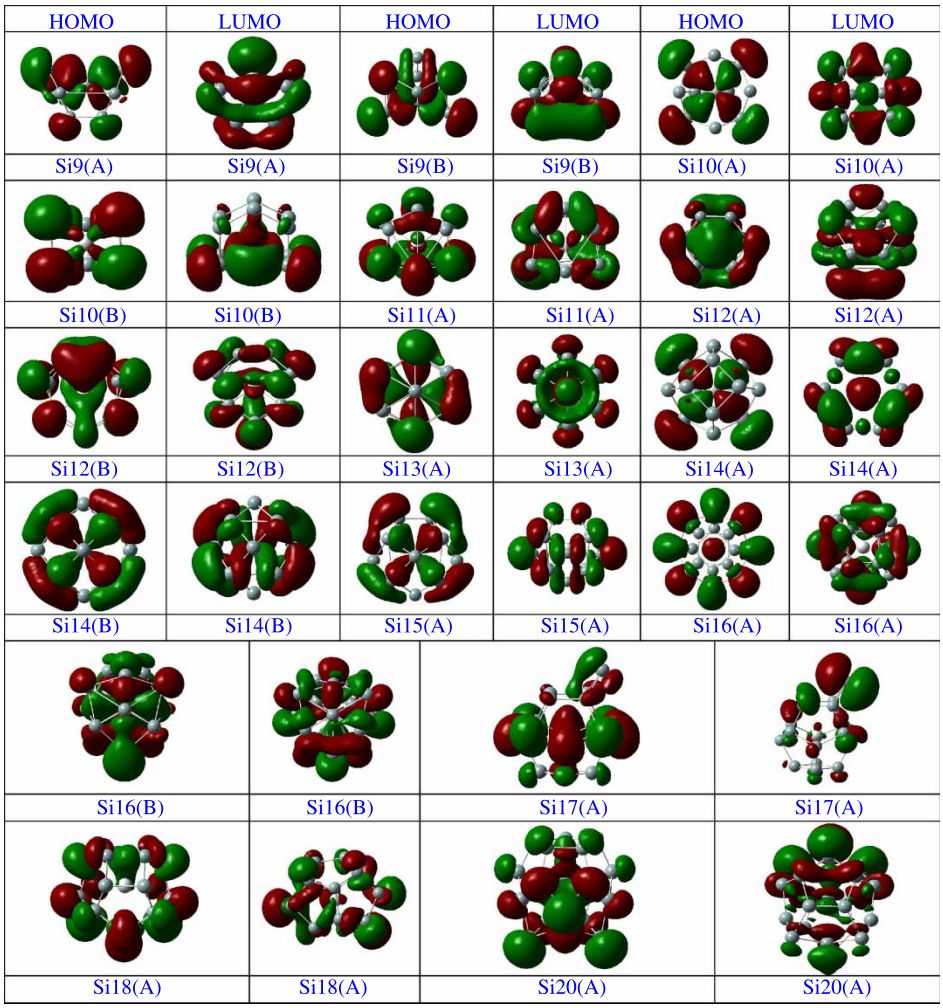

Figure 3. HOMO–LUMO distributions of titanium-doped silicon clusters.

Si atoms in the two hexagons is like half-crossed bonding with a slight rotation about the common axis of the tube passing through the encapsulated Ti and capped Si atoms. The doped cluster has band gap value of 2.33 eV and better stability when compared with the undoped Si13(A) cluster. Other parameters related to the doped clusters are given in Table 2. HOMO–LUMO distributions of the ground-state capped structure is shown in Figure 3. Both HOMO and LUMO are distributed symmetrically about the capped silicon atom. The LUMO distribution is mostly inside the cluster. As with other doped clusters, here also the guest atoms are negatively charged. The meaning of the negative charge on the doped atom is the charge transfer from the cage to the guest atom. This indicates favourable endohedral doping of the TM atoms in the cluster.

3.1.8 n = *14*

Three different optimised structures are calculated in Si14 nanoclusters. The ground-state structure Si14(A) is a combination of six pentagons and three isolated quadrilaterals. This combination gives higher stability to any cluster as discussed before. This is true in case of Si14(A) cluster also and hence it gives ground-state cluster. The other two structures contain approximately the same amount of optimisation energy. Si14(B) contains four quadrilaterals of average bond length 2.72 Å with a band gap of 1.01 eV. Both Si14(B) and Si14(C) structures are bicapped hexagonal prism structure with a B.E. 4.13 per atom and zero dipole moment. The capped Si atom is not at the centre of the hexagons but is displaced symmetrically. The ground-state structure Si14(A) has a HOMO–LUMO gap of 1.96 eV with a B.E. slightly higher than the first two structures with an amount 4.27 eV. The first two structures can easily accommodate a single TM atom inside with more stability when compared with the undoped structures. The optimised Ti-encapsulated Si14 structures, Si14(A)Ti and Si14(B)Ti, are shown in Figure 2. Si14(A)Ti structure has a large dipole moment value of 1.11 D. The HOMO–LUMO gap of this cluster

is lower (1.15 eV) when compared with the other isomer Si14(B)Ti. The Si–Si bond in Si14(A)Ti varies between 2.33 and 2.76 Å, whereas the same in Si14(B)Ti varies from 2.51 to 2.93 Å. These are the first cage clusters that can absorb the guest atom endohedrally. The ground-state structure Si14(A)Ti is similar to the undoped Si14(A) structure. But the doped structure is symmetrical because the doped TM atom can absorb the unsaturated silicon dangling bonds from the surface of the cage and reduce the stain acting on the cage surface. This is the first fullerene-like structure. Due to the relatively bigger size and the nature of HOMO orbital distribution, this cage can endohedrally dope a number of TM atoms. In the present work, only three TM atoms are reported.

3.1.9 n = *15*

In Si15 series, three different kinds of optimised structures are obtained as shown in Figure 1. These two structures can be obtained after small modification in Si14 clusters. Si15 clusters are having almost the same amount of optimisation energy and same amount of HOMO–LUMO gap of 2.22 eV. The average B.E. per atom of the atoms in the clusters of this series is higher than Si14 clusters and is of value 4.22 eV. The doped Si15 cluster is shown in Figure 2. It has a dipole moment of 0.727 D and band gap value of 2.25 eV. It has more stability than the undoped structures. The calculated single optimised structure of Si15(A)TM is quite similar to Si14(A)TM. It is easy to understand the structure of Si15(A)TM by adding one Si atom to the bottom of the rhombi in Si14(A)TM. The optimised structure shows that it has 2 pentagons and 10 rhombi. Two pentagons are interconnected by one of their common arm and are also connected to six other rhombi. It has an average dipole moment of 0.52 D and an average band gap of 2.25 eV. Both Si14(A)TM and Si15(A)TM can be taken as 'bag' kind of structure. The size of the optimised cage structure increases with the doping from Ti to Hf and with a concomitant increase in the bond lengths. The HOMO distribution of Si15(A)Ti cluster is very similar to Si14(B)Ti HOMO distribution. The distribution inside is symmetrical about the doped atom; on the cage surface it is extended more on the top side of the cluster as shown. Therefore, the dipole moment of this cluster is higher than the Si14(B)Ti cluster.

3.1.10 n = *16*

Three different kinds of pure and corresponding Ti-doped Si16 clusters are calculated and are shown in Figures 1 and 2, respectively. Comparing the optimised energies of the structures, it is found that the doped clusters are much more stable than the undoped clusters. Among the undoped clusters, the ground-state Si16(A) structure is more stable than the other two clusters, with a B.E. of 4.33 eV and HOMO–LUMO gap of 1.84 eV, which is relatively low. The other two structures have higher band gap values of 2.12 eV and B.E. of 4.28 eV. The different parameters of these clusters are presented in Table 1. Doping of Si16 clusters with different TM atoms gives more symmetrical and stable clusters. Doped cluster, Si16(A)TM, a fullerene-like cage structure with D_{4d} symmetry, is a ground-state cluster. Si16(B)TM also has a similar football-like structure with optimum energy close to Si16(A)TM, but Si16(C)TM has asymmetrical structures with relatively less stability than Si16(A)TM and Si16(B)TM. In Si16(A)TM structure, two rhombi are widely separated. It has eight more pentagons also. Each rhombus is connected to four pentagons separately and gives a symmetrical structure. The combination of pentagons and squares reduces the strain in this structure and gives a stable fullerene-like isomer. In order to further check the global optimisation of this structure, re-optimisation has been done after a little distortion of the previously obtained geometry. This has been done for other clusters also. The isomer Si16(B)TM has a football-like structure with a relatively low value of B.E. compared with the fullerene isomer Si16(A)TM. Both the structures can be obtained by adding two silicon atoms with Si14(A)TM and Si14(B)TM, respectively. HOMO–LUMO distribution of Si16(A)Ti and Si16(B)Ti is shown in Figure 3. The HOMO distribution in Si16(A)Ti is symmetrical about the doped atom with an empty space between the inside and outside distributions. Due to the relatively bigger space inside the cluster and strong bonding between the silicon atoms, it can absorb a number of elements inside.

3.1.11 n = *17*

This cluster is just a little modification of the Si16(A) cluster with an additional silicon atom with one arm of the rhombus as shown in Figure 1. In the present calculation, there is only one Si17 cluster found. It has B.E. slightly higher than the average B.E. of Si16 clusters of value 4.32 eV and has a small band gap of energy 1.83 eV. The doped structure is similar to TM-doped Si16(A) structure as shown in Figure 2 except the additional silicon atom. It has a high dipole moment of value 1.746 D and a band gap of energy 1.962 eV. The HOMO orbital distribution is similar to Si16(A)Ti with the exception of some additional distribution surrounding the last silicon atom in the cage.

3.1.12 n = *18 and 19*

The optimised structures of both the Si18(A) and Si19(A) clusters are distorted with almost the same amount of B.E. as Si16 and Si17 pure clusters of value 4.33 eV. By removing two silicon atoms from Si18(A), one can

easily obtain the structure of Si16(A) cluster. Pure Si19(A) does not have any symmetrical structure. It has higher B.E. of value 4.36 eV with a small value of band gap as shown in Table 1. Both the clusters can absorb TM atoms endohedrally, but this doping cannot give symmetrical structure. The optimised structure of Si18(A)TM is a combination of one hexagon with two rhombi connected to its two arms. Out of eight pentagons, four pentagons are connected to the remaining four arms of the hexagon. The other four pentagons were used to close the upper part of the structure and give a cage-like structure. It has an average dipole moment of 0.70 D, which is close to the dipole moment of Si17(A)TM. The optimised Si19(A)TM structure does not give any symmetrical cage with relatively low value of B.E. compared with the clusters with $n = 16–18$ and 20.

3.1.13 n = *20*

This is the last member of this series in the present calculations. Two different kinds of optimised structures are found in the present calculations. The undoped cage-like structure is a little modification of Si19(A) cluster with higher value of B.E. that gives more stability and symmetry than the Si19(A) cluster. Si20(B) is a tube-like structure with an average diameter of 7.15 Å. TM-doped optimised Si20(A) cluster is shown in Figure 2. The size of the cage cluster is bigger than undoped Si20(A) cluster with the increasing value of the average bond lengths. The bond length of undoped cluster varies from 2.22 to 3.12 Å, whereas in the case of undoped cluster it varies from 2.30 to 2.57 Å. The doped cage structure has a dipole moment 1.66 D and of band gap 1.61 eV. The dipole moment of the doped cluster is much higher than the undoped cluster. It is observed that in all cage-like structures doping of TM atoms always increases the cage size and gives more stability to the structures in comparison with the undoped structure. The fullerene-like structure of Si20(A)TM is more symmetrical than Si19(A)TM. The size of this cage cluster is bigger than other Si(n)TM clusters with increasing value of the average bond lengths. The optimised structure has an average dipole moment of 3.58 D and a band gap of 1.48 eV. The optimised Si20(A)TM structure contains 12 pentagons and none of them are in a single plane. This structure is not as symmetrical as Si20H20 reported by Kumar and Kawazoe [19]. The addition of hydrogen atoms to the silicon atoms in the Si(n)M clusters terminates the dangling bonds of silicon and gives a more symmetrical structure after balancing the strain acting between different pentagons. In Si(n)TM clusters, except for $n = 14$ and 16, the strain acting between pentagons or between pentagons and squares distorts the cage structure. This is also reflected in the vibrational spectrum of the clusters. The distorted structure always gives a greater number of vibrational modes, hence a relatively greater number of vibrational frequencies in comparison with the symmetrical fullerene structures and these will be discussed in the next section. Since the clusters with $n = 18–20$ are not symmetrical, their HOMO–LUMO distributions are also distorted. But all of these clusters can endohedrally absorb a number of guest elements due to the bigger cage size.

3.2 Binding Energy (B.E.), stability (ΔE^n), HOMO–LUMO gap (ΔE), Ionization Energy (I.P.), electron affinity (E.A.), chemical potential (μ), charge transfer and vibrational spectra of the optimised clusters

The B.E. curve of the optimised clusters is shown in Figure 4. The B.E. of the cages has been defined with respect to the free silicon and TM atoms present in the respective clusters. The variation of the average as well as the B.E. of the ground-state pure clusters shown in Figure 4(a) increases with the number of silicon atoms present in the cluster. It is to be noted that both the curves shown in Figure 4(a) show three local maxima at $n = 12$, 14 and 16. Stability graph of the ground-state pure clusters in different charged states shown in Figure 5 also supports the nature of variation of the B.E. of pure clusters. From the stability graph of the pure clusters, the magic nature of the neutral clusters for $n = 14$ and 16 remains magic in charged states also. Comparing the pure silicon clusters with

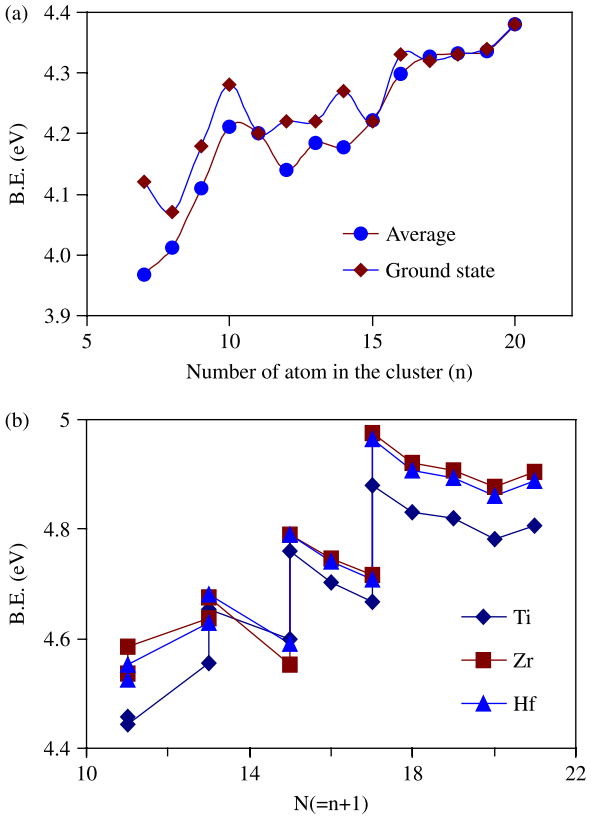

Figure 4. Variation of B.E. with the size of the clusters: (a) pure and (b) doped.

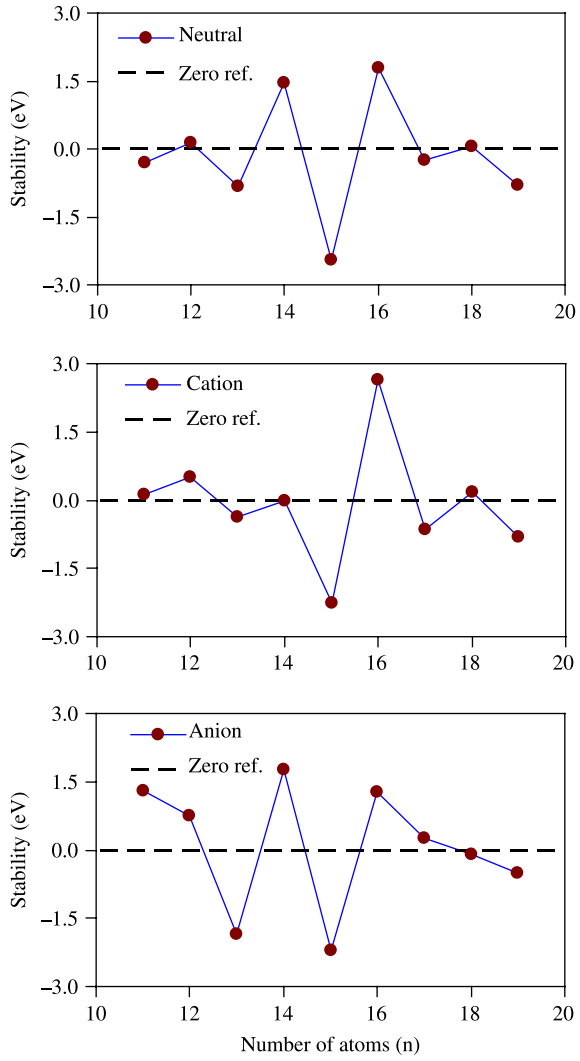

Figure 5. Variation of stability of ground-state pure silicon clusters in different charged state.

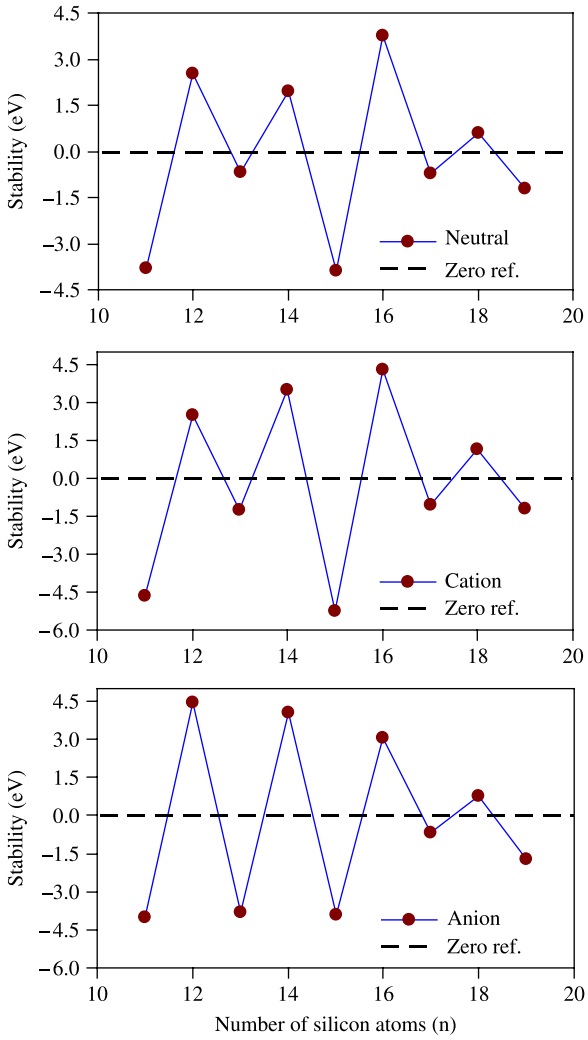

Figure 6. Variation of stability of ground-state titanium-doped silicon clusters in different charged state.

the titanium-doped clusters, it could be found that the variation of B.E. in the doped clusters are much more regular and higher than the pure clusters for same value of n. In the doped clusters, the B.E. also shows a local maximum for the ground-state clusters with $n = 12$, 14 and 16 in the B.E. graph shown in Figure 4(b). Stability graphs of the titanium-doped ground-state clusters (Figure 6) in different charged states also support the B.E. behaviour as like in the pure clusters. The optimised structures of the doped clusters shown in Figure 2 show that the ground-state-doped clusters for $n = 12$, 14 and 16 are very much symmetrical in comparison with their other isomers and also to their neighbouring clusters. As stated in the previous section, the doped TM atoms absorb the unsaturated dangling bonds present on the surface of the titanium cages and give more stability. Among all the structures from $n = 10$–20, the Figure 5(b) shows that the ground-state Si16(A)Ti has the maximum B.E. per atom. This is because of the combination different pentagons and isolated rhombi in the cluster that reduces the strain acting in the bonds and gives higher stability to this cluster. Variation of stability in doped clusters is more regular than the pure clusters. The clusters with an even number of silicon atoms in the clusters are all magic and these clusters remain magic in the charged states also. In the present report, the nature of the variation of B.E. with the number of atoms in the clusters is different from that reported by Kawamura et al. [24]. In a recent study, it has been reported that in hydrogenated Si cages, B.E. monotonically increases up to $n = 20$ and then there is a slight decrease [25]. In the present calculation, B.E. of the clusters with $n > 16$ decreases slightly up to $n = 19$. The nature of all B.E. curves are the same and are independent of the type of doping in the clusters. B.E. of Zr-doped clusters is always higher in comparison with the

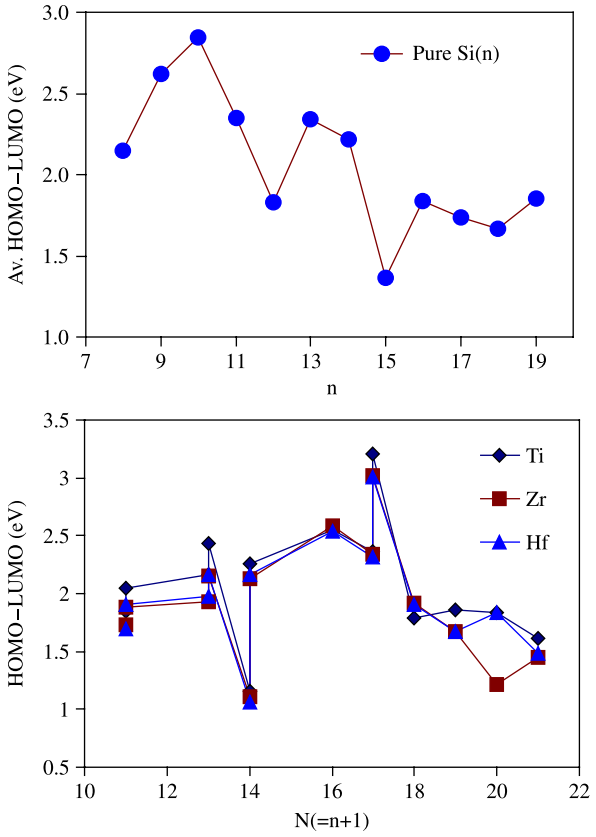

Figure 7. Variation of HOMO–LUMO gap with the size of the pure and doped clusters.

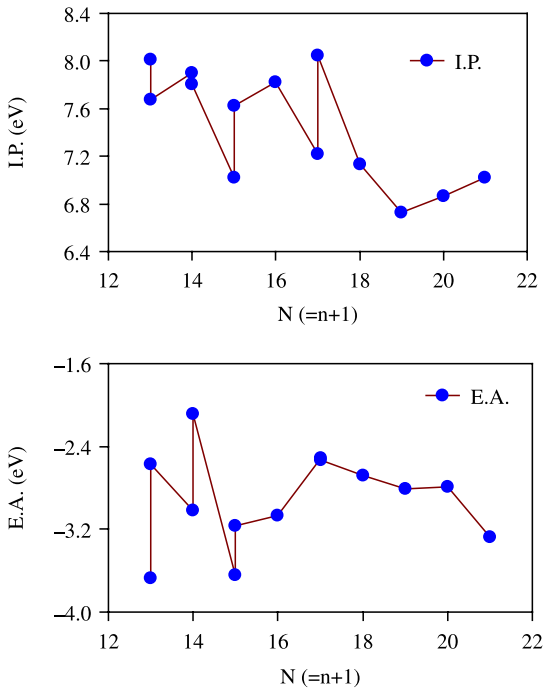

Figure 8. Variation of I.Ps. and E.A. of the titanium-doped clusters.

other metal doping in a particular geometry. On the basis of this behaviour, one can expect that the cages for $n = 14$ and 16 would show strong abundance in the experiment. Experimentally also it has been found that Si16(A)Ti has more abundance than the other geometries [17–19].

Variations of average HOMO–LUMO gap (ΔE) of both pure and doped clusters are shown in Figure 7. The average HOMO–LUMO gap (ΔE) of the pure silicon clusters first increases with the size of the clusters and shows a maximum value close to 3.0 eV. The ground-state cluster for $n = 10$ also shows a maximum value of 3.01 eV. The HOMO–LUMO gap then decreases and shows a two more local maxima at $n = 13$ and 16. The average HOMO–LUMO gap in pure clusters varies from 1.30 to 2.9 eV. On the other hand, in doped clusters the HOMO–LUMO gap varies from 1.6 to 2.7 eV with the size of the cluster. The HOMO–LUMO gap shows local maxima for the ground-state isomers with $n = 12$, 14 and 16. The HOMO–LUMO gap variation has a local maximum value (1.26 eV) for cage with $n = 19$. Since the variation of HOMO–LUMO gap is almost independent of the internal metal doping and also it is small in the whole range of study,

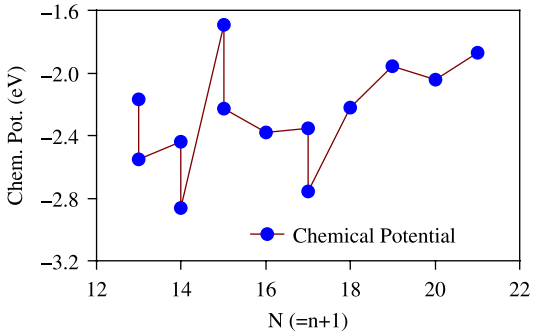

Figure 9. Variation of chemical potential with N in the Ti-doped clusters.

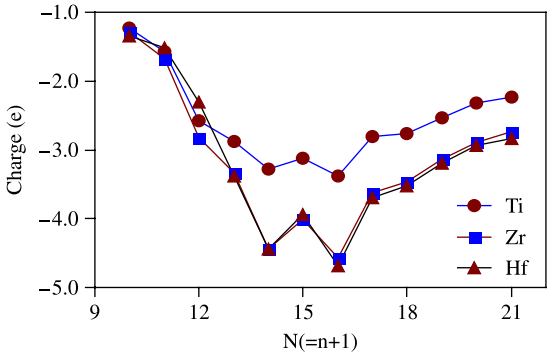

Figure 10. Variation of charge on different doped elements in the clusters.

therefore, metal-doped silicon clusters could be an interesting sample even with a mixture of clusters of different sizes may have similar optical properties. The variation of HOMO–LUMO gap in doped clusters also indirectly supports the B.E. and stability graph of the neutral clusters. Higher HOMO–LUMO gap means less activity in chemical reactions and hence indirectly behaves as stable cluster. The clusters with $n = 12$, 14 and 16 all therefore can be taken as relatively stable clusters in comparison with the other doped clusters.

To check the stability of the clusters, second-order energy difference $\Delta E^n = E(n+1) + E(n-1) - 2E(n)$ (or stability) is also calculated for both the pure and doped clusters. To check the stability in charged states, variation of stability of the clusters for $n = 10$–20 in different charged states is also calculated for ground-state clusters. The variation of stability with n is shown in Figure 5 (for neutral ground-state and corresponding charged clusters) and Figure 6 (for Ti-doped neutral ground-state and corresponding charged clusters). According to the data

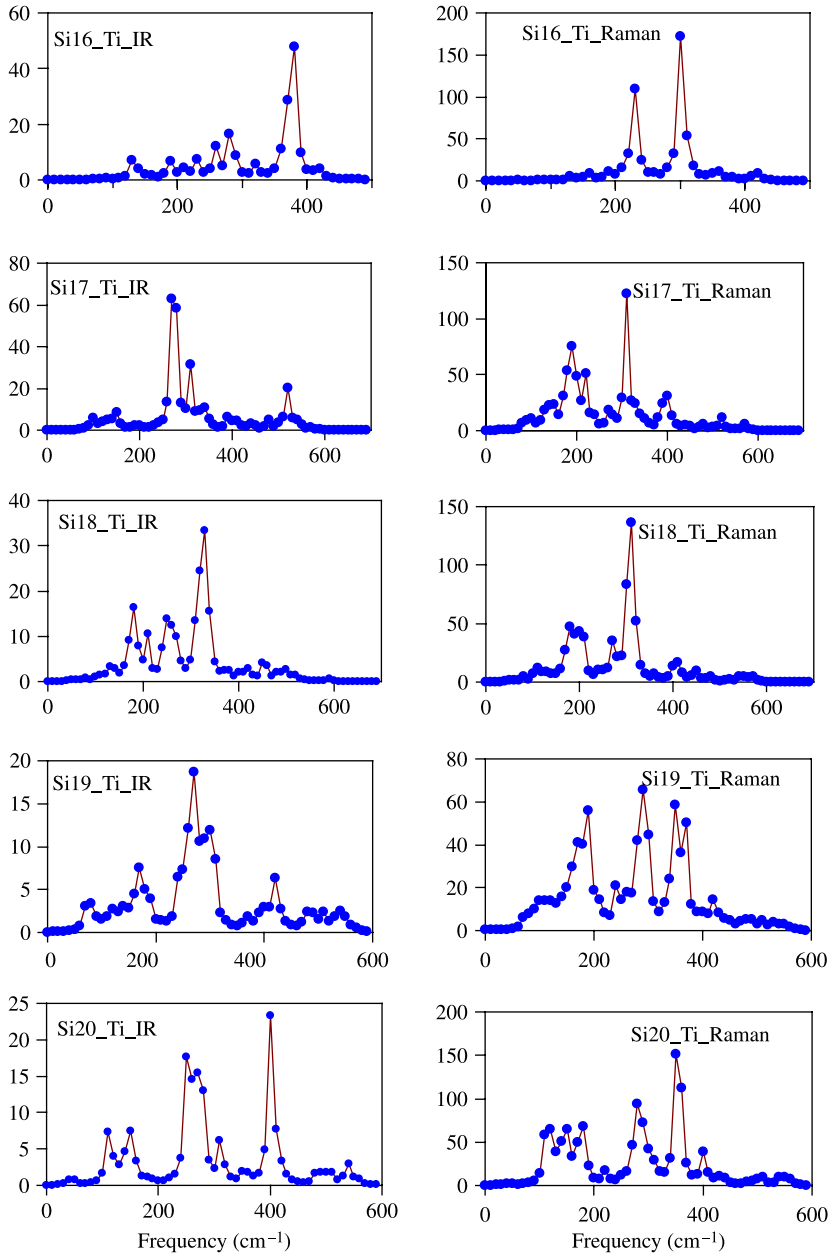

Figure 11. IR and Raman spectrum of some selected titanium-doped silicon clusters. The vertical axis represents the IR intensities or Raman activities in arbitrary units.

of second-order difference, ΔE^n, of the Ti-doped clusters calculated by Kawamura et al. [25], clusters with $n + 1 = 11$ and 13 are found stable (or magic). But this is not supported by experiment. This could be due to the quick reactive nature of these clusters because of higher E.A. In the present calculation the cluster with $n = 12$ is also found magic in neutral as well as in charged states. To verify the stability of the doped neutral clusters, I.P., E.A. and chemical potential of all isomers are calculated and their variations with the size of the clusters are shown in Figures 8 and 9. For the most stable Si16(A)Ti in this series shows that I.P. is relatively higher than the other clusters, whereas the chemical potential ($\mu = -$(I.P. + E.A.)/2) shows a minimum. Higher I.P. indicates the stability of the cluster in neutral state and minimum chemical potential reflects the inactive nature of the cluster in reaction. E.A. value of this cluster has an average value.

Variation of the charge carried by the doped TM atoms in the clusters shows identical behaviour and is presented in Figure 10. With the increase of the size of the cluster, the amount of negative charge on the doped atom increases and shows a minimum values at $n = 14$ and 16. This behaviour also supports the nature obtained from the variation of other physical parameters of the clusters to support the stable nature of the clusters with $n = 14$ and 16. Increase of the negative charge on the doped atom in the cluster is basically reflecting an increase of binding nature between the cage and the doped atom or, in other words, increases of embedding energy of the system. It has already been discussed that the clusters for $n = 14$ and 16 have magic nature and their B.E. is also higher than the other structures. The variation of charge on the doped atom with the size of the cluster also supports this. For $n > 16$, the charge on the doped atoms decreases, which means that the stability of the cluster for $n = 16$ is maximum.

Optical properties of the clusters are tested by calculating the vibrational (IR) and Raman spectra of the optimised geometries and are presented in Figure 11 only for titanium-doped clusters within the range of $n = 16$–20. The absence of imaginary frequency in the spectrum and the nature of stability, chemical potential, etc., of the clusters represent the stable nature of the clusters. The dominant peaks shown in the IR spectrum is due to the vibration of the metal atom in the silicon cage, whereas the vibration of the silicon cage mainly contributes to the Raman activity. Raman activity mainly corresponds to the breathing mode and in this mode all silicon atoms in the clusters move together without any relative phase difference between them. In case of highly symmetric clusters, like Si14(A)Ti and Si16(A)Ti, the number of modes in the Raman spectrum is less than the clusters with relatively less symmetry. The number of modes present in Raman spectrum of the above two clusters are much less than the other clusters.

4. Conclusions

In summary, the study of the electronic structures and stabilities of pure and TM (Ti, Zr and Hf)-doped silicon clusters is presented. Different properties of the pure and metal-doped optimised geometries of the clusters, like binding energies, stabilities, HOMO–LUMO gap, electron affinities, I.Ps., charge transfer, IR and Raman spectra, particularly for titanium-doped silicon clusters, are discussed. Based on the results, the following conclusions can be made:

(1) Both in pure and doped clusters, the B.E. per atom of the clusters increases with the increase in the number of atoms in it. For the same size of clusters, B.E. is more in symmetric clusters, like Si14(A)TM and Si16(A)TM. With further increase in the size ($n > 16$), the B.E. slightly decreases and then again it has a tendency to increase both in pure and in doped clusters. Among the structures with $n < 16$, Si14(A)TM has a relatively higher B.E. Higher B.E. in symmetric fullerene-like clusters Si14(A)TM and Si16(A)TM indicates that the structures with combination of pentagons and rhombi reduce the strain in the cluster and give more stability. This is supported by the calculated stabilities of the doped clusters in different charged states and also by the variation of negative charge transfer from the cage to the doped atoms in the clusters.

(2) With the increase of the size of the clusters, the HOMO–LUMO gap shows a maximum at Si16(A)TM. Higher value of HOMO–LUMO gap indicates the higher value of I.P. and this is also supported by the variation of I.P. with the size of the cluster. Nearly the same value of the average HOMO–LUMO gap for different n and TM is interesting as samples even with a mixture of clusters of different sizes may have similar optical properties.

(3) With the increase in the number of the atoms in the clusters, chemical potential shows a minimum at $n = 16$ for Si16(A)Ti fullerene isomer. This shows that the reactive nature of the clusters is minimum for $n = 16$ in fullerene-like isomer. Therefore, the chemical potential and stability curves support the stable nature of Si16(A)TM cluster. From the stability curve, it has been found that the doped clusters with $n = 12$, 14 and 16 are always magic in all charged states. The variations of stabilities of the pure and doped clusters in different states show that the TM-doped clusters are more stable than the pure silicon clusters. Hence, experimental abundance of these clusters is higher than the other geometries in experiment.

(4) IR intensities and Raman activities show distinct spectra for different optimised clusters. This also reflects the change of bonding nature with the size

of the clusters. This can be useful to identify the structures of these clusters from experiments. IR and Raman spectra do not show any imaginary frequency in the optimised geometries. Moreover, it shows that the number of modes present in the Raman spectrum in symmetric clusters is less compared with the less symmetric clusters.

References

[1] K. Pradhan and P. Sen, *First principles study of Sc, Ti, and V doped Na_n (n = 4,5,6) clusters: enhanced magnetic moments*, Phys. Rev. B 77 (2008), 045408.

[2] V. Kumar and Y. Kawazoe, *Magic behavior of $Si_{15}M$ and $Si_{16}M$ (M = Cr, Mo, and W) clusters*, Phys. Rev. B 65 (2002), 073404.

[3] H. Hiura, T. Miyazaki, and T. Kanayama, *Formation of metal-encapsulating Si cage clusters*, Phys. Rev. Lett. 86 (2001), pp. 1733–1736.

[4] V. Kumar and Y. Kawazoe, *Metal-encapsulated fullerene like and cubic caged clusters of silicon*, Phys. Rev. Lett. 87 (2001), 045503.

[5] V. Kumar and Y. Kawazoe, *Metal-doped magic clusters of Si, Ge, and Sn: the finding of a magnetic superatom*, Appl. Phys. Lett. 83 (2003), pp. 2677–2679.

[6] V. Kumar, C. Majumder, and Y. Kawazoe, *$M@Si_{16}$, M = Ti, Zr, Hf: π conjugation, ionization potentials and electron affinities*, Chem. Phys. Lett. 363 (2002), pp. 319–322.

[7] V. Kumar and Y. Kawazoe, *Hydrogenated silicon fullerenes: effects of H on the stability of metal-encapsulated silicon clusters*, Phys. Rev. Lett. 90 (2003), 055502.

[8] V. Kumar and Y. Kawazoe, *Metal-encapsulated caged clusters of germanium with large gaps and different growth behavior than silicon*, Phys. Rev. Lett. 88 (2002), 235504.

[9] V. Kumar and Y. Kawazoe, *Magnetism in clusters of non-magnetic elements: Pd, Rh, and Ru*, Eur. Phys. J. D, 21 (2003), pp. 81–84.

[10] J. Lu and S. Nagase, *Structural and electronic properties of metal-encapsulated silicon clusters in a large size*, Phys. Rev. Lett. 90 (2003), 115506.

[11] F. Hagelberg, C. Xiao, and W.A. Lester, Jr., *Cagelike Si_{12} clusters with endohedral Cu, Mo, and W metal atom impurities*, Phys. Rev. B 67 (2003), 035426.

[12] S.N. Khanna, B.K. Rao, and P. Jena, *Magic numbers in metallo-inorganic clusters: chromium encapsulated in silicon cages*, Phys. Rev. Lett. 89 (2002), 016803.

[13] P. Sen and L. Mitas, *Electronic structure and ground states of transition metals encapsulated in a Si_{12} hexagonal prism cage*, Phys. Rev. B 68 (2003), 155404.

[14] S.N. Khanna, B.K. Rao, P. Jena, and S.K. Nayak, *Stability and magnetic properties of iron atoms encapsulated in Si clusters*, Chem. Phys. Lett. 373 (2003), pp. 433–438.

[15] V. Kumar, T.M. Briere, and Y. Kawazoe, Ab initio *calculations of electronic structures, polarizabilities, Raman and infrared spectra, optical gaps, and absorption spectra of $M@Si_{16}$ (M = Ti and Zr) clusters*, Phys. Rev. B 68 (2003), 155412.

[16] Z. Chen, A. Hirsch, S. Nagase, W. Thiel, and P. von Rague Schleyer, *Spherical sila- and germa-homoaromaticity*, J. Am. Chem. Soc. 125 (2003), pp. 15507–15511.

[17] M. Ohara, K. Miyajima, A. Pramann, A. Nakajima, and K. Kaya, *Geometric and electronic structures of terbium–silicon mixed clusters ($TbSi_n$; $6 \le n \le 16$)*, J. Phys. Chem. A 106 (2002), pp. 3702–3705.

[18] M. Ohara, K. Koyasu, A. Nakajima, and K. Kaya, *Geometric and electronic structures of metal (M)-doped silicon clusters (M = Ti, Hf, Mo and W)*, Chem. Phys. Lett. 371 (2003), pp. 490–497.

[19] S.M. Beck, *Mixed metal–silicon clusters formed by chemical reaction in a supersonic molecular beam: implications for reactions at the metal/silicon interface*, J. Chem. Phys. 90 (1989), pp. 6306–6312.

[20] T.-C. Tsai, L.-Z. Yu, and C.-T. Lee, *Electroluminescence emission of crystalline silicon nanoclusters grown at a low temperature*, Nanotechnology 18 (2007), 275707.

[21] D. Comedi, O.H.Y. Zalloum, E.A. Irving, J. Wojcik, T. Roschuk, M.J. Flynn, and P. Mascher, *X-ray-diffraction study of crystalline Si nanocluster formation in annealed silicon-rich silicon oxides*, J. Appl. Phys. 99 (2006), 023518.

[22] L. Liu, C.S. Jayanthi, and S.-Y. Wu, *Factors responsible for the stability and the existence of a clean energy gap of a silicon nanocluster*, J. Appl. Phys. 90(8) (2001), pp. 4143–4151.

[23] V. Kumar and Y. Kawazoe, *Hydrogenated caged clusters of Si, Ge, and Sn and their endohedral doping with atoms:* ab initio *calculations*, Phys. Rev. B 75 (2007), 155425.

[24] H. Kawamura, V. Kumar, and Y. Kawazoe, *Growth, magic behavior, and electronic and vibrational properties of Cr-doped Si clusters*, Phys. Rev. B 70 (2004), 245433.

[25] H. Kawamura, V. Kumar, and Y. Kawazoe, *Growth behavior of metal-doped silicon clusters Si_nM (M = Ti,Zr,Hf; n = 8–16)*, Phys. Rev. B 71 (2005), 075423.

[26] D. Bandyopadhyay, *A density functional theory-based study of the electronic structures and properties of cage like metal doped silicon clusters*, J. Appl. Phys. 104 (2008), 084308.

[27] K. Burke, J.P. Perdew, and Y. Wang, *Electronic Density Functional Theory: Recent Progress and New Directions*, J.F. Dobson, G. Vignale, and M.P. Das, eds., Plenum, New York, 1998.

[28] J.P. Perdew, J.A. Chevary, S.H. Vosko, K.A. Jakson, M.R. Pederson, D.J. Singh, and C. Fiolhais, *Atoms, molecules, solids, and surfaces: applications of the generalized gradient approximation for exchange and correlation*, Phys. Rev. B 46 (1992), pp. 6671–6687.

[29] J.P. Perdew, J.A. Chevary, S.H. Vosko, K.A. Jakson, M.R. Pederson, D.J. Singh, and C. Fiolhais, *Erratum: atoms, molecules, solids, and surfaces: applications of the generalized gradient approximation for exchange and correlation*, Phys. Rev. B 48 (1993), p. 4978.

[30] J.P. Perdew, in *Electronic Structure of Solids '91*, P. Ziesche and H. Eschrig, eds., Akademie Verlag, Berlin, 1991.

[31] J.P. Perdew, K. Burke, and Y. Wang, *Generalized gradient approximation for the exchange-correlation hole of a many-electron system*, Phys. Rev. B 54 (1996), pp. 16533–16539.

[32] J.G. Han and F. Hagelberg, *A density functional investigation of $MoSi_n$ (n = 1–6) clusters*, J. Mol. Struct.: Theochem 549 (2001), pp. 165–180.

[33] C. Adamo and V. Barone, *Exchange functionals with improved long-range behavior and adiabatic connection methods without adjustable parameters: the mPW and mPW1PW models*, J. Chem. Phys. 108 (1998), pp. 664–675.

[34] J. Wang and J.G. Han, *Geometries, stabilities, and electronic properties of different-sized $ZrSi_n$ (n = 1–16) clusters: a density-functional investigation*, J. Chem. Phys. 123 (2005), 064306.

[35] P. Guo, Z.Y. Ren, F. Wang, J. Bian, J.G. Han, and G.H. Wang, *Structural and electronic properties of $TaSi_n$ (n = 1–13) clusters: a relativistic density functional investigation*, J. Chem. Phys. 121 (2004), pp. 12265–12275.

[36] M.J. Frisch, G.W. Trucks, H.B. Schlegel, G.E. Scuseria, M.A. Robb, J.R. Cheeseman, V.G. Zakrzewski, J.A. Montgomery, Jr., R.E. Stratmann, J.C. Burant, et al., *Gaussian 98, Revision A.9*, Gaussian, Inc., Pittsburgh PA, 1998.